Thermocapillary and thermoelectric effects in liquid lithium plasma facing components

M.A. Jaworski [a,*], N.B. Morley [b], D.N. Ruzic [a]

[a] University of Illinois at Urbana-Champaign, 104 S. Wright St., Urbana, IL 61801, USA
[b] MAE Department, University of California, Los Angeles, CA 90095-1597, USA

ARTICLE INFO

ABSTRACT

Recent experiments have renewed interest in the use of liquid lithium as a plasma facing component (PFC). The liquid metal surface will experience a number of effects which are considered in the present work with simple analytical and more complete computational models. These include the thermal response under fusion relevant heat loads causing thermocapillary and thermoelectric effects. Analytical solutions for simplified flow are given showing the surface velocity of these liquid metals due to thermocapillary effects in conjunction with magnetohydrodynamic drag. A parameter describing dominant conduction or convection is developed which shows that thin-films relevant to NSTX will be conduction dominated. Thermoelectric effects could propel liquid lithium with velocities of 10 s of cm/s providing a significant boost to energy transport.

© 2009 Elsevier B.V. All rights reserved.

1. Introduction

Recent experiments have shown improvements in plasma performance with the use of liquid lithium plasma facing components. Most recently, the CDX-U device operated with a large area (2000 cm^2) liquid lithium limiter [1,2]. Among the reported results are an increase in the measured energy confinement time over the ITER98P ELMy H-mode scalings [1], a reduction in MHD activity, and strong density control [2]. Previously, "supershot" regimes had been reported with lithium wall conditioning in the TFTR machine [3,4].

Several laboratory experiments have examined lithium pumping [5–7]. Baldwin et al. showed that lithium absorbs deuterium until converted into lithium deuteride [7] and Sugai showed impurity gettering [6]. Both of these studies explain density control and low Z_{eff} on CDX-U and TFTR. McCracken showed a temperature dependence in hydrogen ion trapping efficiency which may affect the performance of liquid lithium PFCs [5]. In addition to reduced trapping, evaporation may occur. Liquid lithium is viable in a temperature range between 180 °C and about 350–400 °C. The lower bound is the melting temperature of lithium [8] while the upper temperature is determined by acceptable evaporation rates for the machine being studied [9].

The free-surface lithium limiter of CDX-U absorbed a power flux of 60 MW/m^2 from an e-beam without significant evaporation [2]. This result was achieved by passive pumping of the lithium by thermocapillary effects [10]. These flows are created by gradients in the surface tension along a free-surface of a fluid. The effects of magnetic fields on the fluid flow has been examined in crystal growth experiments [11] but there is limited study of the effect in the context of fusion [2,12]. Shercliff showed that the thermoelectric effect could induce flows in conjunction with a magnetic field. A dissimilar metal pairing combined with a temperature gradient induces thermoelectric currents. The resultant $\vec{J} \times \vec{B}$ force accelerates the fluid. These flows are referred to as thermoelectric magnetohydrodynamic (TEMHD) [13]. Bulk fluid motion resulting from these effects can enhance heat transfer or result in fluid ejection from the restraining surface. Table 1 shows typical divertor heat fluxes and heat flux gradients in experiments indicating the magnitude of values considered in the present study.

This paper presents scaling studies of thermocapillary and thermoelectric flows in the presence of a magnetic field. The studies are carried out in support of experiments at the University of Illinois on the Solid/Liquid Lithium Divertor Experiment (SLiDE) [12] and the upcoming Liquid Lithium Divertor on NSTX [14]. The SLiDE experiment will examine power loading of a free-surface liquid lithium tray in a varying magnetic field at normal incidence. Divertor and first-wall PFCs will have an oblique-incidence magnetic field so both cases are modeled. An analysis of the relevant heat transfer regimes is shown in Section 2 and order of magnitude scales are given in Section 3. Computational results are shown in Section 4 and a discussion follows.

---

* Corresponding author.
  E-mail address: mjaworsk@uiuc.edu (M.A. Jaworski).

Table 1
Summary of peak heat flux and peak heat flux gradient of selected fusion experiments.

Machine	$q_{max} \frac{MW}{m^2}$	$\frac{dq}{dx} \frac{MW}{m^2-m}$
DIII-D	5	45 [21]
JET	15	186 [22]
JET (ELMs)	90	1300 [22]
NSTX	10	100 [23]

2. General considerations

In the case of fluid motion, both conduction and convection are present. The following 0th order analysis shows when conduction, convection, or both effects must be considered.

Fig. 1 shows a simple control volume (CV). The fluid temperature rises under the action of an applied heat flux such that the temperature difference applicable to both conduction and convection is simply $\Delta T = T_1 - T_0$. Heat leaves the CV via convection and conduction. In the case of a porous material, conduction occurs in both the liquid and solid leading to an *effective* thermal conductivity [15] given as $k_{eff} = fk_l + (1 - f)k_s$ where l and s subscripts refer to the liquid and solid, respectively, and f is the porosity of the material. This energy balance is written in Eq. (1) as follows:

$$Q_{in} = k_{eff}A_n\frac{\Delta T}{a} + \rho_l c_{p,l}A_t\Delta Tu, \tag{1}$$

where k is the fluid thermal conductivity, $A_n = Lz$ is the surface area normal to the incident flux, $A_t = az$ is the tangential area, ρ is the fluid density, c_p is the fluid specific heat and u is the mean velocity.

A comparison between the conduction and convection terms can be seen by rearranging Eq. (1) against the nominal conduction:

$$\frac{q_{in}}{k_{eff}\Delta T/a} = 1 + \frac{f\rho_l c_{p,l}}{k_{eff}}\frac{a^2u}{L} = 1 + \xi, \tag{2}$$

where $\alpha = k/\rho c_p$ is the thermal diffusivity, and q_{in} is the input heat flux. Only the liquid convects energy, so while the saturated material's effective conductivity is in the denominator, the effective thermal diffusivity of the saturated material is not used. A dimensionless variable, ξ is introduced to represent the ratio of convective heat transfer to conduction. When $\xi \ll 1$ heat transfer is conduction dominated. For cases when $\xi \gg 1$ it is convection dominated. These ranges are shown in Fig. 2 for different velocities and thicknesses. In the case of the porous medium, a porous molybdenum foam with 80% porosity saturated with liquid lithium at 250 °C is used [15].

3. Reduced dimensionality analyses

In the case of unidirectional, surface tension driven flow with a normal incidence magnetic field, an analytical solution to the flow field is available [12]. This magnetic geometry is applicable to initial SLiDE experiments. The solution for the velocity as a function of depth is given as follows:
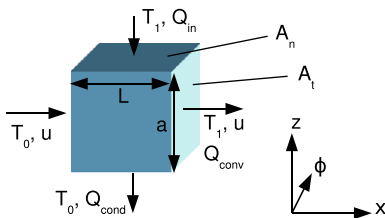

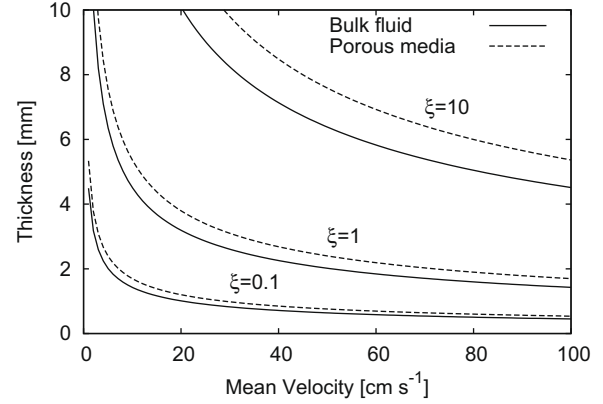**Fig. 1.** Power balance in a small control volume.

Fig. 2. Values of ξ for 100% liquid (solid line) and 80% liquid (dashed line) porous materials as a function of mean flow velocity and material thickness. Values of $\xi < 0.1$ indicate conduction dominated heat transfer while $\xi > 10$ indicates convection dominated heat transfer.

$$u(z^*) = \frac{\gamma a^2}{\mu k_l}\frac{\partial q_{in}}{\partial x}\frac{\sinh(Ha z^*)}{Ha \cdot \cosh(Ha)}, \tag{3}$$

where γ is the surface tension temperature dependence coefficient, $\partial q/\partial x$ is the surface tangential heat flux gradient, μ is the dynamic viscosity and z^* is the dimensionless height from the bottom surface of the fluid. Ha denotes the Hartmann number. The sinh velocity profile indicates that only a thin surface layer is moving as Ha increases. In the case of steady conduction from the top surface to the bottom, a linear temperature gradient exists in the fluid. As an approximation this linear gradient is assumed for the present analysis and a temperature weighted mean velocity is defined as follows:

$$\bar{u} = \int_0^1 u(z^*)\Theta(z^*)dz^*, \tag{4}$$

where $\bar{u}_{wt}$ is the weighted mean velocity, and $\Theta(z^*)$ is the weighting function. In the case of a linear weighting function $\Theta(z^*) = z^*$, the resulting mean velocity is given in Eq. (5):

$$\bar{u}_{wt} = \frac{\gamma a^2}{\mu k}\frac{\partial q_{in}}{\partial x}\frac{Ha \cdot \cosh(Ha) - \sinh(Ha)}{Ha^3\cosh(Ha)}. \tag{5}$$

In the case of a 0.13 T field normal to a 10 mm deep pool with and incident 10^8 W/m² · m heat flux gradient (*c.f.* Table 1), the mean velocity is 0.5 cm/s for weighted and unweighted averages.

TEMHD effects have been previously analyzed in the literature [13]. In this case a toroidal field (*i.e.* ϕ in Fig. 1) is assumed present (SLiDE models a poloidal field). If the primary temperature gradient in the material is due to conduction of energy from the plasma facing surface to the back wall (*i.e.* along z in Fig. 1) then the temperature gradient relevant to TEMHD flow can be represented with the incident heat flux and effective conductivity yielding the following:

$$\bar{u}_{TEMHD} = r_pP\left(\frac{\sigma}{\mu}\right)^{1/2}\frac{Ha - \tanh(Ha)}{Ha(Ha + C\tanh(Ha))}\frac{q_{in}}{k_{eff}}, \tag{6}$$

where P is the thermoelectric power of the metal pair, r_p is the average pore size, and σ is the fluid electrical conductivity. The constant $C = (\sigma r_p)/(t\sigma_w)$ is the ratio of impedances in the fluid and solid, where t is the wall thickness and σ_w is the wall resistivity. This flow is directed perpendicular to both the temperature gradient and magnetic field. For reference, the mean pore size of the material reported in Ref. [15] is estimated at 400 μm with a ligament thickness of about 100 μm. Using the properties of molybdenum and liquid lithium, an NSTX level field of 0.5 T and a surface heat flux of 1 MW/m², the mean velocity is 28 cm/s.

4. Computational simulations

Numerical simulations in 2D and 3D have been carried out for both thermocapillary and TEMHD driven flows and compare well with the analyses described above. These analyses were performed with modified version of the numerical tools described in Ref. [16–19]. In particular, a traction surface boundary condition proportional to the temperature gradient [20] was introduced in the HIMAG code [16–18] to account for thermocapillary forces, and a novel thin wall TE boundary condition was introduced to the 2D model [19] to include the effect of TE currents. Both analyses calculate the heat transfer self-consistently. Detailed results will be reported elsewhere, but a particular example of the effect of field inclination on surface tension gradient driven flows is described below.

A surface heat flux stripe q_{in} = $10^4 \cos(\pi x)\,(1 - U[|y| - 4.5])$ (here x and y are in cm) is applied at the free surface located at z = 1 cm at time t = 0 s. The bottom wall is isothermal and all other walls are adiabatic. Note that since the problem is symmetric that only the $x > 0$ half is simulated in all cases. Case 1 uses a purely toroidal $(\vec{B} = B_y)$ field of 0.5 T. Case 2 also uses a 0.5 T field, but inclined by 15° from the surface. Case 3 utilizes a purely poloidal $(\vec{B} = B_z)$ field of 0.13 T. Note that B_z is the same magnitude in cases 2 and 3 (see Fig. 3).

A 3D image of case 1 is shown in Fig. 4. The formation of a main vortex driven by the surface tension gradient is clearly seen along with other minor vortices. These minor vortices and transport along them disapp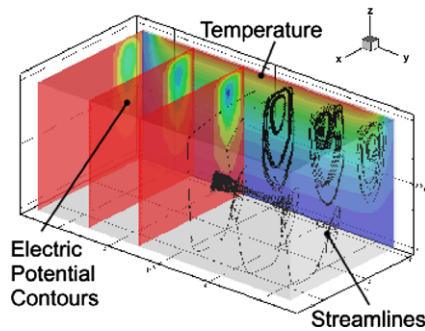ear in case 3 (poloidal field) and flow is similar to Eq. (3). The streamlines around the vortices have an helical nature indicating that while the dominant motion is around the field lines, there is slow circulation inward from the walls and outward from the center along these vortices. The time-dependent, peak surface velocities and temperatures are shown in Fig. 4. The time to reach a steady-state velocity is ≈1 s while thermal development time is slightly longer.

5. Discussion

The regions shown in Fig. 2 and the analysis in Section 3 indicate that the SLiDE device and the present NSTX LLD design will exhibit different behaviors. SLiDE will examine surface-tension driven flows in magnetic fields up to 0.1 T [12] with variable depths of fill enabling access to regions of $\xi \approx 1$. This will provide validation of thermal transport codes describing these flows. For purely surface tension driven flows, the present LLD design will remain in the conduction dominated heat transfer regime due to the thin-films currently planned. There remains a possibility that TEM-HD effects will drive a flow in the thin, porous layer of plasma-sprayed molybdenum material such as is planned in the LLD. Until a film thickness is determined, the impact of this remains unknown. The effectiveness of TEMHD to drive flow indicates the possibility of use in novel divertor, first-wall and blanket module designs.

The simulation peak surface velocities in Fig. 4 decrease with an increasing poloidal field component but the temperature rise does not change significantly from about 1 °C. This indicates that these particular test problems are in the conduction dominated regime (see Fig. 2). It is also interesting to note that the peak surface velocity for the inclined field case matches more closely to the purely surface normal field case 3 of equivalent magnitude (a similar behavior was noted in Ref. [19]). This indicates that for thin-films, the surface normal field orientation currently available in SLiDE may be more representative of true NSTX operation than a simulation experiment with a purely toroidal magnetic field.

6. Conclusion

Analysis of heat transfer modes expected in present liquid lithium systems has been presented. Conduction is expected to be the dominant mode for thin-films such as found on the LLD, while the SLiDE device will enable exploration of regimes where convection is significant. The computational simulations exhibit behavior in accord with the analytical model. Further, 3D computational simulations indicate that it is the surface normal component of the field which determines flow velocity. The ability of the TEMHD effect in a porous material indicates that it may provide an effective method of transporting lithium in fusion relevant conditions and will be the subject of future work.

Acknowledgement

Fig. 3. 3D velocity streamlines (right), contours of electric potential (left), and temperature (back) for a surface heated tray of lithium in a horizontal magnetic field (case 1).
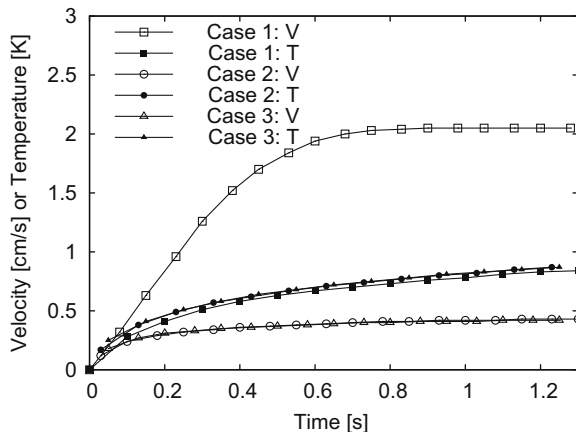

Fig. 4. Peak surface velocities and temperatures for three test cases with different magnetic field inclinations.

References

[1] R. Majeski et al., Phys. Rev. Lett. 97 (2006) 075002.
[2] R. Kaita et al., Phys. Plasmas 14 (2007) 056111.
[3] J.D. Strachan et al., Phys. Rev. Lett. 58 (10) (1987) 1004.
[4] J.A. Snipes et al., J. Nucl. Mater. 196–198 (1992) 686.
[5] G.M. McCracken, S.K. Erents, British Nuclear Energy Society, UKAEA Culham Laboratory, 1969.
[6] H. Sugai et al., J. Nucl. Mater. 220–222 (1995) 254.

 [7] M.J. Baldwin et al., Nucl. Fusion 42 (2002) 1318.
 [8] M.A. Abdou et al., Tech. Rep. UCLA-ENG-99-206, University of California, Los Angeles, November 1999.
 [9] L.E. Zakharov et al., Fusion Eng. Des. 72 (2004) 149.
[10] V.G. Levich, V.S. Krylov, Annu. Rev. Fluid Mech. 1 (1969) 293.
[11] A. Cröll et al., J. Cryst. Growth 183 (1998) 554.
[12] M.A. Jaworski, D.N. Ruzic, IEEE, Albuquerque, NM, 2007.
[13] J.A. Shercliff, J. Fluid Mech. 91 (1979) 231.
[14] H. Kugel et al., J. Nucl. Mater. 390–391 (2009) 1000.

[15] M.A. Jaworski et al., J. Nucl. Mater. 378 (2008) 105.
[16] M.-J. Ni et al., Fusion Sci. Technol. 52 (2007) 587.
[17] M.-J. Ni et al., J. Comp. Phys. 227 (2007) 174.
[18] N.B. Morley et al., Fusion Eng. Des. 72 (2004) 3.
[19] N.B. Morley, M.A. Abdou, Fusion Technol. 31 (1997) 135.
[20] L.Q. Tang, T.T.H. Tsang, Int. J. Numer. Meth. Fluids 28 (1998) 983.
[21] C.J. Lasnier et al., Nucl. Fusion 38 (1998) 1225.
[22] T. Eich et al., J. Nucl. Mater. 313–316 (2003) 919.
[23] V.A. Soukhanovskii et al., J. Nucl. Mater. 337–339 (2005) 475.